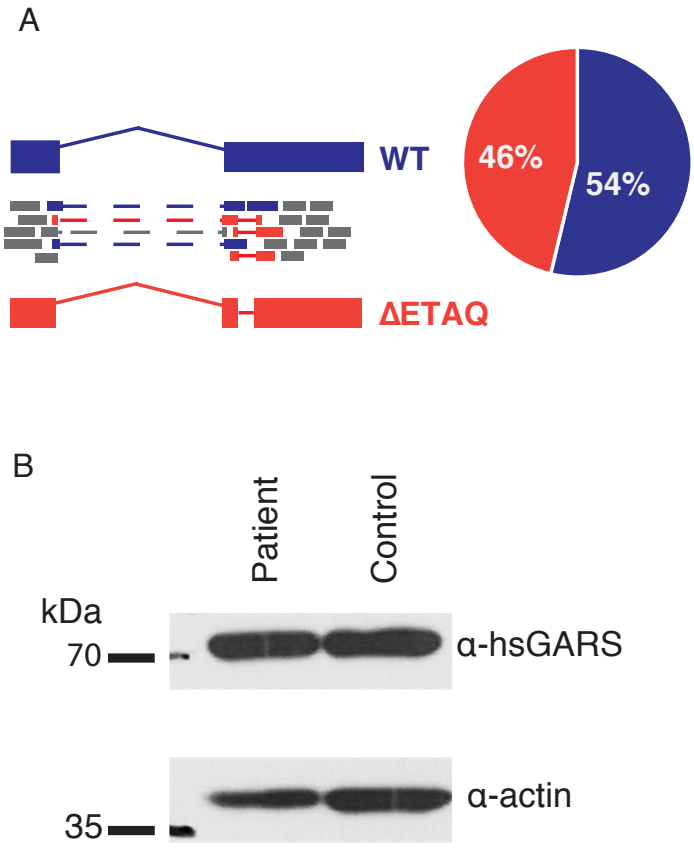

Supplemental Figure 1. The ΔETAQ *GARS* mutation does not affect gene expression.
(**A**) RNA and cDNA libraries were generated from patient fibroblasts. Subsequently, RT-PCR products spanning the mutation were subjected to deep-sequencing analysis. A cartoon representing the *GARS* exon7-exon8 junction is shown with the wild-type (blue) and mutant (red) PCR products indicated. Mapped sequence reads were deemed informative if they spanned the nucleotides affected by the mutation. Of the informative reads, 53.7% were from wild-type (WT) transcripts and 46.3% were from ΔETAQ *GARS* transcripts. (**B**) Western blot analyses were performed with total protein lysates from fibroblast cell lines from affected (Patient) and unaffected (Control) individuals using an anti-GARS or anti-actin antibody, as indicated. Sample names are across the top and protein size markers (kDa) are indicated on the left.

A

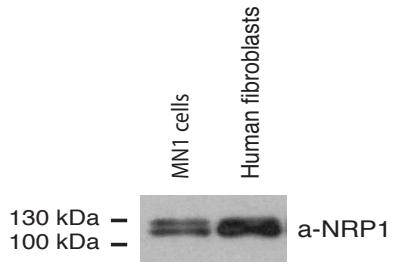

B

	Set 1 WT-1	Set 1 WT-2	Set 1 ΔETAQ-1	Set 1 ΔETAQ-2	Set 2 WT-1	Set 2 WT-2	Set 2 WT-3	Set 2 ΔETAQ-1	Set 2 ΔETAQ-2	Set 2 ΔETAQ-3
GARS_Human	640	398	398	103	1356	1321	2407	957	415	1189
GARS_Mouse	317	210	187	36	646	632	1185	462	215	549
Ratio	2	1.9	2.1	2.9	2.1	2.1	2	2.1	1.9	2.2
NRP1_Mouse	ND	ND	ND	ND	ND	ND	ND	ND	ND	ND

C

	Set 1 Untagged-1	Set 1 Untagged-2	Set 1 Untagged-1	Set 1 Untagged-2	Set 2 Untagged-3
GARS_Human	19	17	123	87	171
GARS_Mouse	5	1	65	46	81
Ratio	NA	NA	1.9	1.9	2.1
NRP1_Mouse	ND	ND	ND	ND	ND

Supplemental Figure 2. The ΔETAQ *GARS* mutation does cause aberrant binding to NRP1.
(**A**) Western blot analyses were performed on total protein lysates from MN1 cells and human fibroblasts using an anti-NRP1 antibody, as indicated. Sample names are across the top and protein size markers (kDa) are indicated on the left. (**B**) Non-normalized spectral counts from mass spectrometry experiments are shown for proteins that co-immunoprecipitated with wild-type (WT) or ΔETAQ GARS; data are shown for human GARS, mouse GARS, and mouse NRP1. The ratio of human:mouse GARS is also provided. Two independent sets of data were generated at two independent institutions, and each set contained two or three biological replicates. ND – not detected. (**C**) Non-normalized spectral counts from mass spectrometry experiments are shown for proteins that co-immunoprecipitated with untagged wild-type GARS; data are shown for human GARS, mouse GARS, and mouse NRP1. The ratio of human:mouse GARS is also provided. Two independent sets of data were generated at two independent institutions, and each set contained two or three biological replicates. NA – not applicable. ND – not detected.

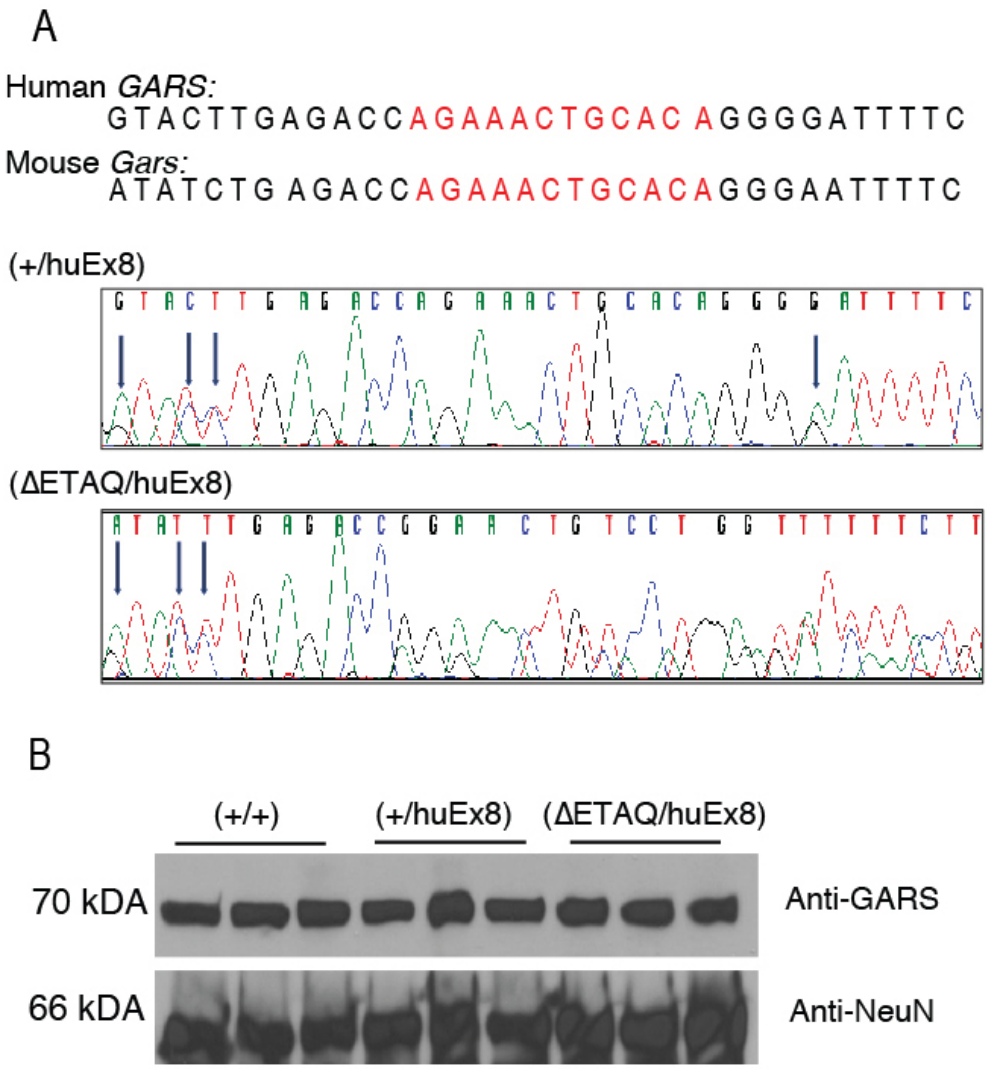

Supplemental Figure 3. **mRNA and protein levels in *Gars*$^{\Delta ETAQ/huEx8}$ mice.** (**A**) Chromatograms from Sanger sequencing analysis of RT-PCR products generated using cDNA isolated from sciatic nerve showing the first 34 bases of *Gars* exon 8 *(n=3 mice per genotype)*. Human-specific nucleotides expressed within *Gars*$^{+/huEx8}$ and *Gars*$^{\Delta ETAQ/huEx8}$ are indicated by arrows. The 12 bp ΔETAQ mutation is highlighted in red in the sequence above and is indicated by double sequence starting at base 13 of the chromatogram. (**B**) Western blot analysis of brain homogenates for GARS expression in the indicated mouse strains. The blot was re-probed with an anti-NeuN antibody to control for variability in protein loading.

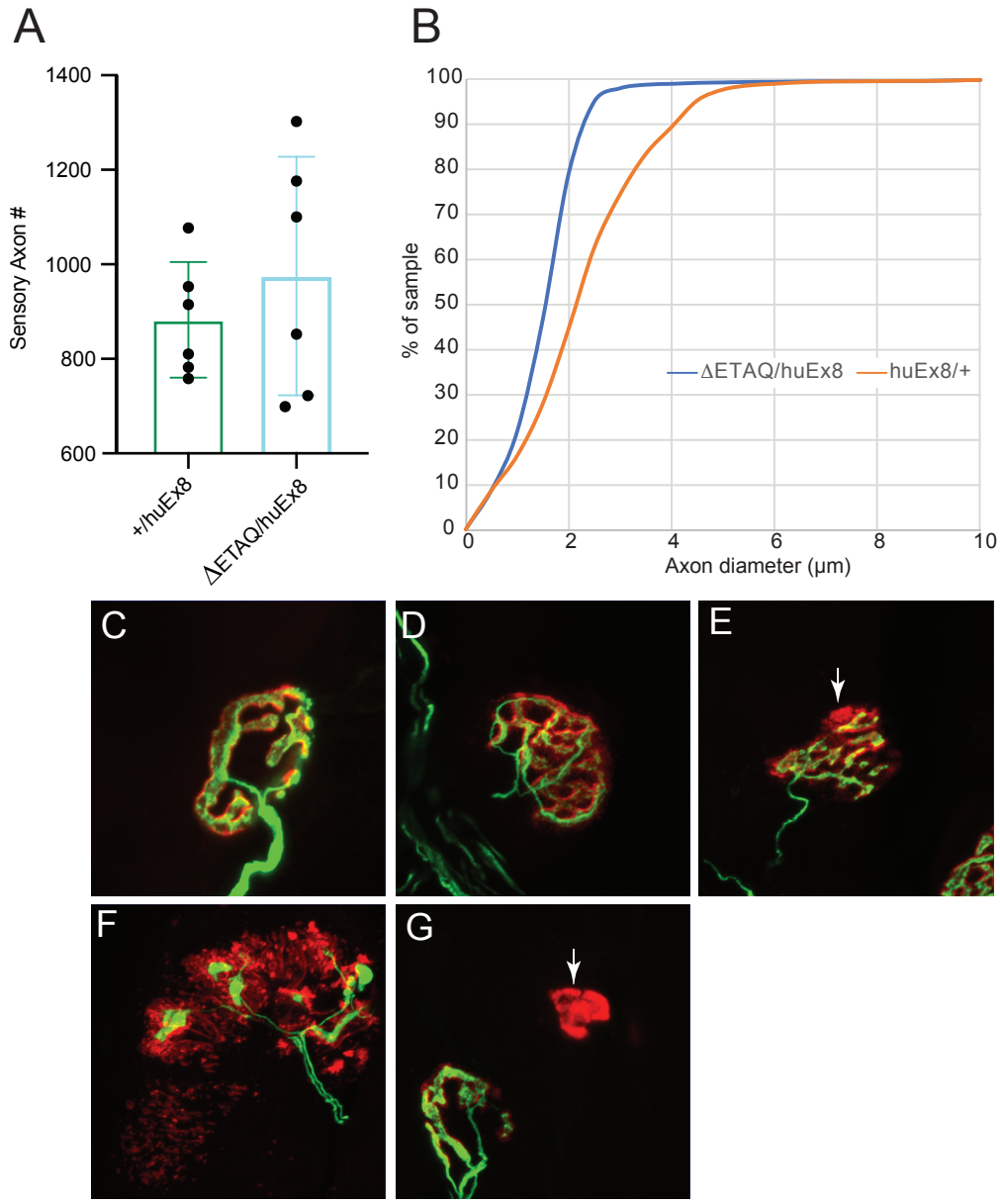

Supplemental Figure 4. *Gars*$^{\Delta ETAQ}$ sensory nerves and neuromuscular junctions (NMJs). The sensory branch of the femoral nerve was evaluated for myelinated axon number and axon diameter at 12 weeks-of-age in 7 *Gars*$^{+/huEx8}$ mice and 8 *Gars*$^{\Delta ETAQ/huEx8}$ mice. **A)** No reduction in axon number was found. **B)** In a cumulative histogram of axon diameters, the *Gars*$^{\Delta ETAQ/huEx8}$ samples are shifted significantly leftwards, indicating smaller axon diameters. Changes in NMJ morphology in the plantaris muscle were evident even at 6 weeks-of-age. **C)** In control mice, the motor nerve terminal (green) completely overlaps the postsynaptic acetylcholine receptors (AChRs, red) and the junction has a complex "pretzel" shape. **D-G)** The *Gars*$^{\Delta ETAQ/huEx8}$ mice show varying degrees of NMJ dysmorphology. **D)** Some junctions are fully innervated, with the nerve overlapping the postsynaptic receptors even if the shape is not as complex or sharply defined as in wild type. **E)** Some partially innervated junctions show only small areas of AChRs without an overlying nerve terminal (arrow). **F)** Other NMJs have dystrophic nerve terminals and large areas of AChR localization with an overlying

nerve terminal. Mild **(E)** to severe **(F)** instances of partial innervation were aggregated as "partial innervation." **G)** AChR plaques in the endplate band with no overlying nerve (arrow) were considered denervated. Note the adjacent innervated junction establishing that nerve staining was otherwise good in this sample. Scale bar = 25 microns in **C-G**.

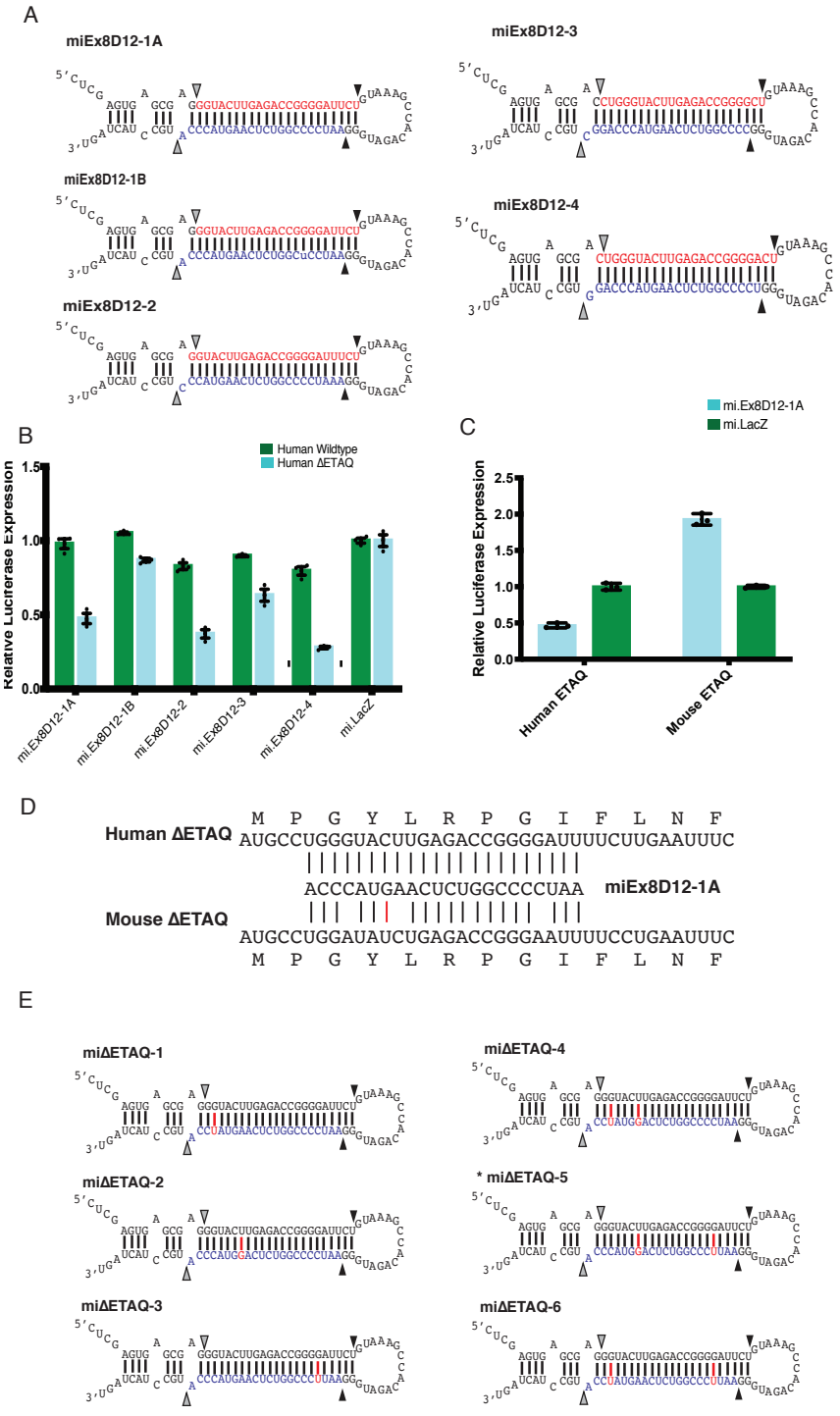

Supplemental Figure 5. **All miRNAs targeting ΔETAQ disease allele tested *in vitro*. (A)** The five miRNAs hairpins originally tested targeting the ΔETAQ mutation in the human *GARS* gene. The guide strand is indicated in blue, and the passenger strand is in red. Gray and black arrowheads indicate the Drosha and Dicer cut sites respectively. **(B)** The first set of miRNAs tested in a dual-luciferase assay. HEK293 cells were cotransfected with a single miRNA and the dual luciferase reporter containing either wild type or ΔETAQ human *GARS* cloned as the 3'UTR of *Renilla* luciferase. Gene silencing was

determined by measuring the ratio of *Renilla* to Firefly luciferase and triplicate data are presented as the average mean ratio ± SEM. Based on the efficient knockdown of the human disease-allele and preservation of the wild type allele, miEx8D12-1A was chosen as the lead candidate. **(C)** The lead candidate miEx8D12-1A was tested in a dual-luciferase assay against the mouse ΔETAQ mutant gene. Despite effective silencing of the human disease allele, it was unable to target the ΔETAQ mouse *Gars* mRNA. Triplicate data were averaged and presented as the mean ± SEM. **(D)** The guide strand of the initial lead miRNA and its complementarity to the target regions of both human and mouse ΔETAQ *Gars*. Base pairing is indicated by vertical lines with G-U bonds shown in red. **(E)** The hairpin structures of six variants of miEx8D12-1A. The guide strand is shown in blue, with the changes to the original miR sequence indicated in red. *In vitro* testing results for these miRNAs is shown in Figure 2. The lead miRNA is marked with an asterisk and was renamed mi.ΔETAQ for all further testing

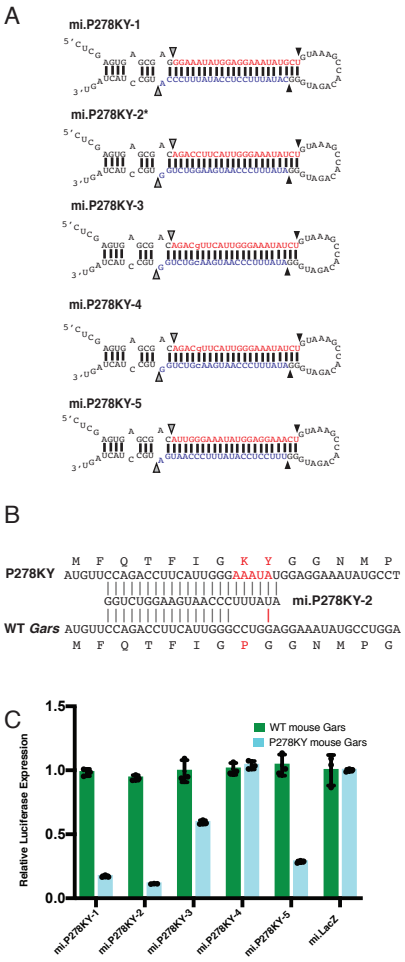

Supplemental Figure 6. U6.miP278KY microRNAs can specifically knockdown P278KY mouse Gars mRNA *in vitro* (A) Hairpin structures of all pre-miRNAs targeting P278KY mouse *Gars* mRNA. The guide strand is shown in blue, while the passenger strand is in red. Drosha and Dicer cut sites are indicated by gray and black arrowheads, respectively. The best performing miRNA *in vitro* is marked with an asterisk and the name was shortened to miP278KY for further testing. **(B)** The sequence of the guide strand of the best performing miP278KY and its complementarity to both wild type and mutant mouse *Gars*. The P278KY mutation is shown in red. Vertical lines indicate the base paring between the miRNA and the target genes, with weaker G-U bonds shown in red. Allele-specificity is achieved by effective base-pairing of the miRNA with the mutant allele, while also having much lower complementarity to the wild type. **(C)** miRNAs were tested *in vitro* by cotransfecting HEK293 cells with a single miRNA and a dual-luciferase reporter containing either wild type or P278KY mouse *Gars* cloned as the 3'UTR of Renilla luciferase. Target gene silencing was determined by measuring the ratio of Renilla to Firefly luciferase. Triplicate data were averaged and presented as the mean ratio ± SEM.

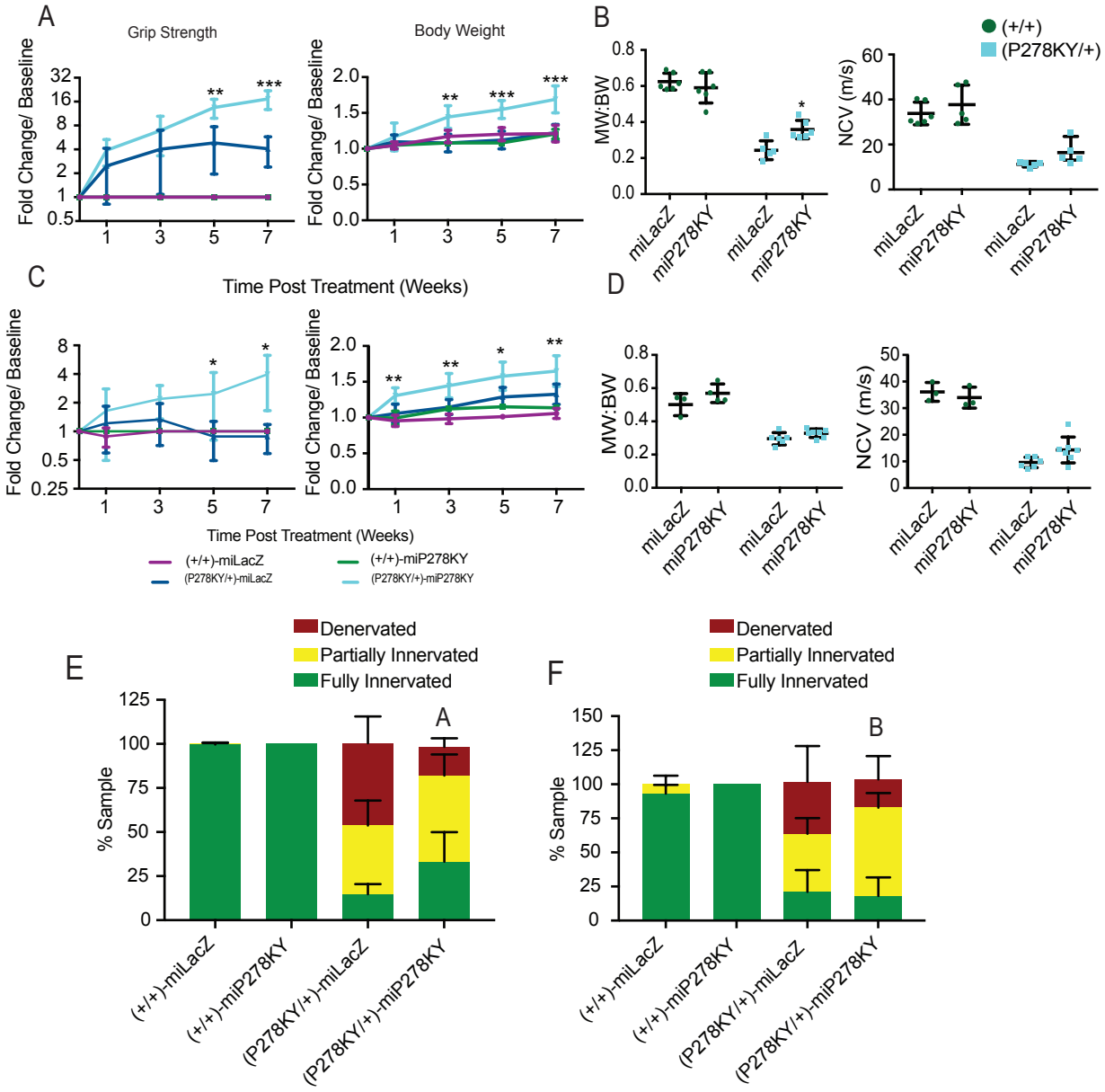

Supplemental Figure 7. Reduction in Mutant *Gars* Expression Also Alleviates Neuropathy in Post-Disease Onset *Gars*$^{(P278KY/+)}$ Mice. (A and C) mi-P278KY treatment at 5 weeks (early onset) or at 9 weeks (late post onset) yields significant increases in grip strength as determined by the wire hang test starting at 5 weeks post treatment in both early- **(A)** and late-symptomatic **(C)** Gars$^{(P278KY/+)}$ mice. Treated P278KY mice also gain weight starting 3 weeks post treatment with early-symptomatic mice **(A)** and 1 week post treatment with late-symptomatic mice **(C)**. When evaluated 7 weeks after treatment, an increase in MW:BW within scAAV9.mi.P278KY early- symptomatic *Gars*$^{(P278KY/+)}$ mice was observed **(C),** although scAAV9.miP278KY treatment was unable to improve NCV within this cohort or MW:BW nor NCVs in the late-symptomatic P278KY mice **(B and D)**. However, scAAV9.miP278KY treatment significantly prevented or reversed NMJ breakdown in both early- and late- symptomatic *Gars*$^{(P278KY/+)}$ mice **(E-F)**. All statistics were completed with a One-Way ANOVA with Tukey Posthoc comparisons. Star represents significance between MiLacZ and MiP278KY-treated Gars$^{P278KY/+}$ mice (* = <0.05 ** =

<0.005 *** =<0.001). A = significant difference in fully innervated NMJs, B = significant difference in partially innervated NMJs. Late-symptomatic Cohort: MiLacZ-treated *Gars*$^{(+/+)}$ n=6, scAAV9.miP278KY-treated *Gars*$^{(+/+)}$ n=5-6, mi.LacZ-treated *Gars*$^{(P278KY/+)}$ n=6, and scAAV9.miP278YK-treated *Gars*$^{(P278KY/+)}$ n=7. Early-symptomatic Cohort: miLacZ –treated *Gars*$^{(+/+)}$ n=3, scAAV9.miP278KY-treated *Gars*$^{(+/+)}$ n=3-4, mi.LacZ-treated *Gars*$^{(P278KY)}$ n=6, and scAAV9.miP278KY-treated *Gars*$^{(P278KY/+)}$ n=7. Values are mean ± S.D.

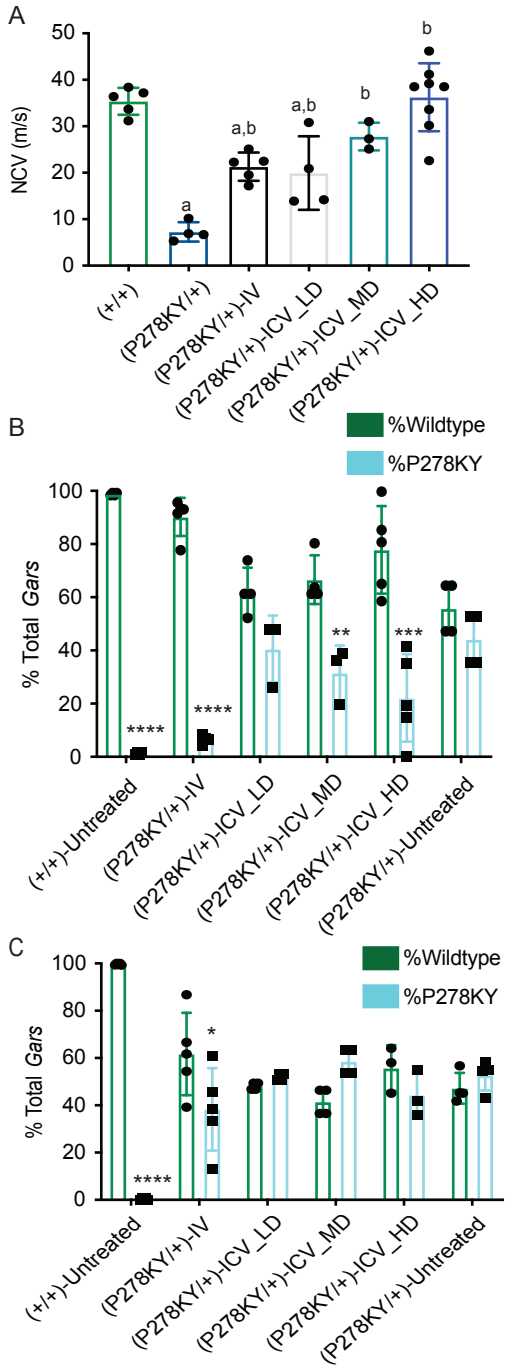

Supplemental Figure 8. Escalating Doses of scAVV9.miP278KY Delivered Via ICV Injection Improves Peripheral Nerve Function in *Gars*$^{(P278KY/+)}$ Mice. (A-B) Significant improvements in nerve conduction velocity correlate with dosage and reductions of mutant *Gars* mRNA expression within dorsal root ganglia when scAAV9.miP278KY was delivered by ICV compared to IV. **(C)** In contrast, these gains in peripheral nerve function did not correlate with reductions in mutant *Gars* expression within liver. N=5 for all experimental groups. IV = intravenous delivery of $1x10^{11}$ vg/mouse, ICV = intracerebroventricular

delivery, LD = low dose of $8.75x10^9$ vg/mouse, MD = median dose of $5.00\ x10^{10}$ vg/mouse, and HD = $1x10^{11}$ vg/mouse. **(A)** Data were analyzed by a One-Way ANOVA followed by Tukey's posthoc comparisons. a = significant from untreated, wildtype control; b = significant from untreated P278KY control. **(B-C)** These data were analyzed with a Two-Way ANOVA with Tukey Posthoc comparisons. Stars represent significance between wildtype and mutant *Gars* expression per experimental group (* = <0.05 ** = <0.005 *** = <0.001 **** = <0.0001). Values are mean ± S.D.

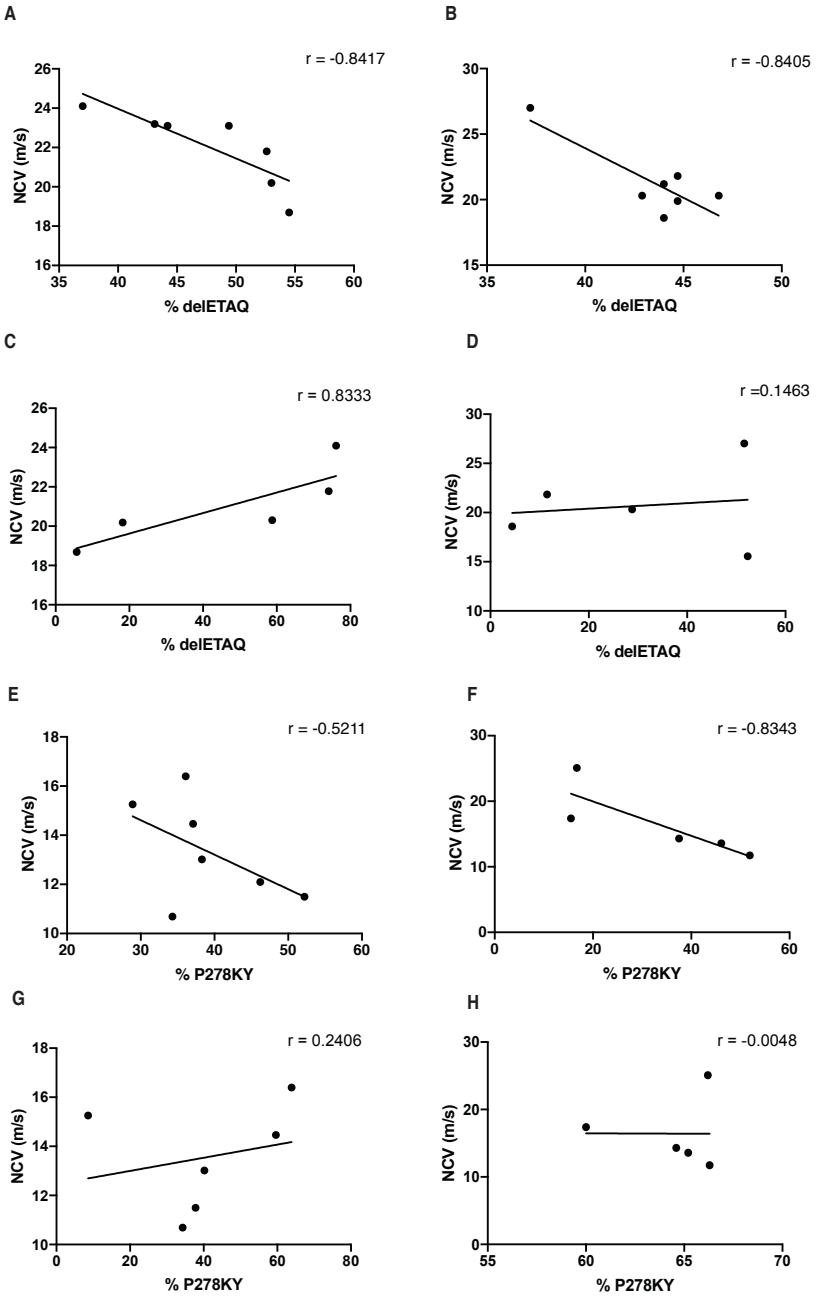

Supplemental Figure 9. Improvements in Phenotype Negatively Correlates With Levels of Mutant *Gars* Expression in Dorsal Root Ganglia (A-B) Scatter plot illustrating the negative correlation between the percentage of the ΔETAQ variant expression within dorsal root ganglia and nerve conduction velocities quantified from scAAV9.mi.ΔETAQ-treated *Gars*$^{(\Delta ETAQ/huEx8)}$ mice within late- **(A)** and early- **(B)** symptomatic cohorts. **(C-D)** Scatter plot illustrating the relationship between the percentage of the ΔETAQ variant expression within liver and nerve conduction velocities quantified from scAAV9.mi.ΔETAQ-treated *Gars*$^{(\Delta ETAQ/huEx8)}$ mice within late- **(C)** and early- **(D)** symptomatic cohorts. **(E-F)** Scatter plot illustrating the negative correlation between the percentage of the P278KY *Gars* variant expression within dorsal root ganglia and nerve conduction velocities quantified from

scAAV9.mi.P278KY-treated *Gars*$^{(P278KY/+)}$ mice within late- **(E)** and early- **(F)** symptomatic cohorts. **(G-H)** Scatter plot displaying the association between the percentage of the P278KY *Gars* variant expression within liver and nerve conduction velocities quantified from scAAV9.mi.P278KY-treated *Gars*$^{(P278KY/+)}$ mice within late- **(G)** and early- **(H)** symptomatic cohorts.

Supplemental Table 1 Kinetic Analysis of Mutant GARS Proteins.

Variant[a]	**k_{cat} (s-1)**	**K_m (µM)**	**k_{cat}/K_m (s^{-1} $µM^{-1}$)**	**Ratio**
Wild-type	0.049 ± 0.014	0.74 ± 0.30	0.066	1
P234KY	0.0012 ± 4.6 x 10^{-4}	8.8 ± 3.3	1.3 x 10^{-4}	1 / 500
ΔETAQ	8.7 x 10^{-6} ± 1.2 x 10^{-6}	1.4 ± 0.085	6.2 x 10^{-6}	1 / 11,000

[a]Human amino-acid positions correspond to GenBank Accession number NP_002038.2

Supplemental Table 2. Effects of scAAV9.mi.ΔETAQ on *In Vivo* GARS Expression in Dorsal Root Ganglia

Age at Injection	Genotype	Treatment	Average Ratio of Mutant: Wildtype *Gars* Expression (± SD)
Neonate (P0-P1)	(huEx8/huEx8)	Untreated	14.0: 86.0 (± 3.28)
Neonate (P0-P1)	(huEx8/huEx8)	sc.AAV9.mi.LacZ	8.0: 92.0 (± 1.275)
Neonate (P0-P1)	(huEx8/huEx8)	sc.AAV9.mi.ΔETAQ	9.6: 90.4 (± 2.07)
Neonate (P0-P1)	(ΔETAQ/huEx8)	Untreated	62.4: 37.6 (± 0.94)
Neonate (P0-P1)	(ΔETAQ/huEx8)	sc.AAV9.mi.LacZ	62.5: 38.6 (± 0.96)
Neonate (P0-P1)	(ΔETAQ/huEx8)	sc.AAV9.mi.ΔETAQ	46.9: 53.1 (±4.79)
5 Weeks	(huEx8/huEx8)	sc.AAV9.mi.LacZ	9.6: 90.4 (± 2.53)
5 Weeks	(huEx8/huEx8)	sc.AAV9.mi.ΔETAQ	8.3:91.7 (± 2.92)
5 Weeks	(ΔETAQ/huEx8)	sc.AAV9.mi.LacZ	63.9: 36.1 (± 3.13)
5 Weeks	(ΔETAQ/huEx8)	sc.AAV9.mi.ΔETAQ	47.2: 52.8 (± 7.88)
9 Weeks	(huEx8/huEx8)	sc.AAV9.mi.LacZ	10.3: 89.7 (± 3.04)
9 Weeks	(huEx8/huEx8)	sc.AAV9.mi.ΔETAQ	6.0: 94.0 (± 1.33)
9 Weeks	(ΔETAQ/huEx8)	sc.AAV9.mi.LacZ	59.3:40.7 (± 6.45)
9 Weeks	(ΔETAQ/huEx8)	sc.AAV9.mi.ΔETAQ	45.3:54.74 (±6.02)

Supplemental Table 3. Effects of scAAV9.miP278KY on Allele-Specific GARS Expression in Dorsal Root Ganglia

Genotype	Treatment	Dose: Route of Delivery	Average Ratio of Mutant:Wildtype *Gars* Expression (± SD)
(+/+)	Untreated	NA	1.2: 98.8 (± 0.43)
(+/+)	sc.AAV9.mi.LacZ	$1x10^{11}$ DRPS/animal: ICV	1.0: 99.0 (± 0.32)
(+/+)	sc.AAV9.mi.P278KY	$1x10^{11}$ DRPS/animal: ICV	0.2: 99.8 (± 0.22)
(P278KY/+)	Untreated	NA	55.8: 44.2 (±9.93)
(P278KY/+)	sc.AAV9.mi.LacZ	$1x10^{11}$ DRPS/animal: ICV	51.7: 48.3 (± 8.46)
(P278KY/+)	sc.AAV9.mi.P278KY	$1x10^{11}$ DRPS/animal: ICV	22.2: 77.8 (±16.44)
(P278KY/+)	sc.AAV9.mi.P278KY	$5x10^{10}$ DRPS/animal: ICV	33.3: 66.65 (± 9.1
(P278KY/+)	sc.AAV9.mi.P278KY	$8.75\ x10^{9}$ DRPS/animal: ICV	38.5:62.15 (± 8.91)
(P278KY/+)	sc.AAV9.mi.P278KY	$1x10^{11}$ DRPS/animal: IV	9.8:90.2 (±8.22)

ICV = Intracerebroventricular Delivery
IV = Intravenous Delivery
NA = Not Available

Supplemental Table 4. Post Onset Effects of scAAV9.mi.P278KY on *In Vivo* GARS Expression in Dorsal Root Ganglia

Age at Injection	Genotype	Treatment	Average Ratio of Wildtype: Mutant *Gars* Expression (± SD)
5 Weeks	(+/+)	scAAV9.mi.LacZ	1.6: 98.4(± 2.46)
5 Weeks	(+/+)	sc.AAV9.mi.P278KY	0.7: 99.3 (± 0.55)
5 Weeks	(P278KY/+)	sc.AAV9.mi.LacZ	55.0: 45.0 (± 7.26)
5 Weeks	(P278KY/+)	sc.AAV9.mi.P278KY	36.2: 63.8 (± 14.74)
9 Weeks	(+/+)	sc.AAV9.mi.LacZ	0.9: 99.1 (± 0.27)
9 Weeks	(+/+)	sc.AAV9.mi.P278KY	0.0: 100.0 (± 0.00)
9 Weeks	(P278KY/+)	sc.AAV9.mi.LacZ	52.3:47.7 (± 4.64)
9 Weeks	(P278KY/+)	sc.AAV9.mi.P278KY	40.6: 59.4 (± 8.95)